THE JOURNAL OF PHYSICAL CHEMISTRY B

Article

pubs.acs.org/JPCB

A Time-Dependent Density Functional Study of a Non-Aromatic [1.1.1.1.1]-Pentaphyrin and Its Lutetium Complex

Flavio Fortes Ramos Sousa, Angelo Domenico Quartarolo, Emilia Sicilia, and Nino Russo*

Dipartimento di Chimica and Centro di Calcolo ad Alte Prestazioni per Elaborazioni Parallele e Distribuite-Centro di Eccellenza MIUR, Università della Calabria, I-87030 Arcavacata di Rende, Italy

Supporting Information

ABSTRACT: The molecular structures and absorption electronic spectra of two novel phototoxic pentapyrrolic expanded porphyrins (a isopentaphyrin derivative and its lutetium complex) have been studied at the density functional level and its time-dependent extension (TDDFT). The geometries were optimized with three different exchange-correlation functionals (PBE0, B3LYP, and ωB97XD) and the SV(P) basis set plus the pseudopotential method for the complex. With respect to the porphyrin, the structure of [1.1.1.1.1]-pentaphyrin and its lutetium complex are predicted much distorted due to the lack of conjugation. The lowest excitation energy band (experimental at 814 nm) for the free-base isopentaphyrin is well predicted by the ωB97XD at 772 nm. The possible photodynamic reaction mechanisms (types I and II) were studied through the calculation of the electron affinity and ionization potentials in solvent, using the COSMO model.

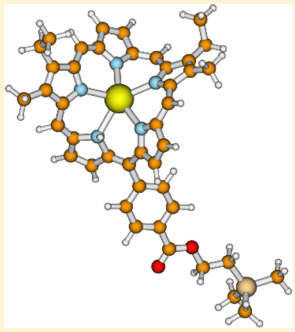

1. INTRODUCTION

Tetrapyrrolic macrocycles are a porphyrin-like class of compounds where the pyrrole rings are held together through *meso*-methine carbon bridges, in a square-planar geometry.[1] The metal-complex form of porphyrins plays a crucial role in many biological processes of life chemistry.[2] Chlorophylls (Mg(II)-chlorin), vitamin B-12 (Co(II)-corrin), and heme (Fe(II)-protoporphyrin) are natural porphyrin complexes essential for plant photosynthesis, oxygen transport in blood, electron transport, and redox catalysis. The spectral features of porphyrins are essentially due to the π-electron conjugation that causes the appearance of absorbing bands in the visible region (400−700 nm).[3] The extension of the macrocycle cavity size with the inclusion of more than four pyrrole subunits brings a new class of polypyrrolic chromophores termed expanded porphyrins.[4,5] The first expanded porphyrin, discovered by Woodward et al. in 1966 but reported with a full characterization only in 1983, was the sapphyrin, a pentapyrrolic macrocycle, whose name was assigned from its color.[6,7] A more general definition of expanded porphyrins, due to Sessler et al., implies the presence of heteroatom rings (thiophene, pyrrole, or furan-like) bonded directly or not through spacers, with at least 17 atoms in the main ring pathway.[8] The nomenclature proposed by Frank and Nonn consists of three parts: (a) the number of π electrons as a prefix in square-brackets; (b) the number of pyrrole units (e.g., pentaphyrin, hexaphyrin); (c) the number of bridging carbons between heteroatom rings in round-brackets.[9] The molecule reported in Figure 1, for example, belongs to the [24] pentaphyrin (1.1.1.1.1) class. The importance of the expanded porphyrins has emerged in different application fields: as photosensitizers in photodynamic therapy (PDT), nonlinear optical materials with large TPA cross sections, near-infrared dyes, contrast agents in magnetic resonance imaging (MRI), and anion recognition sensors.[10−13] The absorption spectra of the expanded porphyrins are generally bathochromically red-shifted with respect to porphyrins because of the increase of the π-electron conjugation length.[4] The enlargement of the inner cavity allows the metal coordination to larger cation ions, than in porphyrins, like lanthanides or actinides.[14] This is the case for the lutetium(III) and gadolinium(III) water-soluble texaphyrin complexes (tripyrrolic penta-aza expanded porphyrins), first synthesized by Sessler et al. in 1993, with a cavity core larger by about 20% than that of porphyrins.[15] These metal complexes are in advanced clinical studies for the PDT treatment of arteriosclerotic disease and as MRI radiation enhancers, respectively. PDT is a light-assisted treatment of tissue lesions and tumors, in which, schematically, a photosensitizer is excited from its ground state S_0 to the first excited state S_1 and then through a radiationless intersystem crossing transition generating the T_1 triplet excited state.[16,17] The electron energy transfer to molecular oxygen ($^3O_2$) can generate the cytotoxic singlet oxygen ($^1O_2$) species (type II PDT mechanism). Another proposed photodynamic action mechanism (type I) is based on the reduction of the photosensitizer in its T_1 state by an organic substrate. The subsequent reaction with $^3O_2$ generates the reactive oxygen species (ROS).[18] The presence of absorption bands, in the so-called therapeutic window (650−800 nm), and the heavy atom in the macrocycle represent some important photochemical features for the design of suitable PDT photosensitizers. In fact, in the first case (red-shifted bands), the radiation allows the treatment of deeper tumors and in the second case (heavy atom presence) the triplet quantum yield can increase because of the intersystem spin

Received: July 10, 2012
Revised: July 31, 2012
Published: August 9, 2012

dx.doi.org/10.1021/jp3068359 | J. Phys. Chem. B 2012, 116, 10816−10823

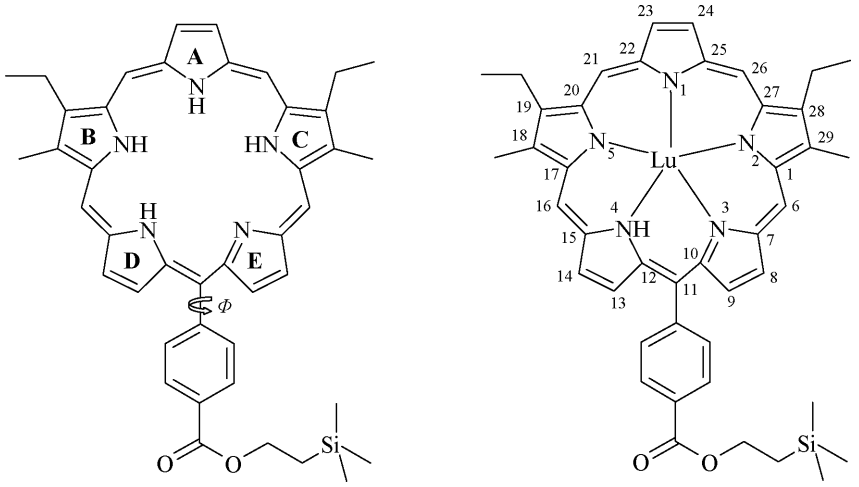

Figure 1. Molecular structures for the isopentaphyrin (**1**) and the lutetium complex (**2**), with atom numbering and ring labeling.

crossing.[19] Recently, the synthesis of a non-aromatic free base expanded pentaphyrin, or 20-[4′-(trimethylsilyl)ethoxycarbonyl]phenyl-2,13-dimethyl-3,12-diethyl-[24] iso-pentaphyrin, its zinc(II) and lutetium(III) complexes have been reported for potential application in PDT.[20] In particular, the lutetium complex showed a great ROS production and phototoxicity in several cancer line cells. In the present theoretical work, we will deal with the ground and excited state properties of these compounds, at the density functional level of theory and its time-dependent formalism, in order to calculate the electronic spectra and characterize their spectral features. Moreover, the basic PDT mechanisms will be investigated, by means of the excited state electron affinities and ionization potential calculations.

2. COMPUTATIONAL DETAILS

Molecular geometry optimization of **1** and **2** structures, in the ground singlet and excited triplet electronic states, was carried out without symmetry constraints at the density functional level of theory. For this purpose, two different kinds of exchange-correlation functionals, belonging to the pure hybrid (a) and long-range corrected hybrid (b) models, were employed: (a) the Becke semiempirical three-parameter gradient corrected (B3LYP)[21] and the parameter-free Perdew−Burke−Erzenrhof (PBE0);[22,23] (b) the ωB97X and ωB97XD functionals.[24,25] The B3LYP and PBE0 functionals contain different amounts of the Hartree−Fock (HF) exact exchange energy (20 and 25%, respectively). The performance of the B3LYP and PBE0 approaches, for the prediction of molecular geometries and optical properties, is well established in the literature, for the study of the ground and excited states of organic and metal-containing systems.[26,27] For the molecular optimizations, the SV(P) split-valence basis set of Ahlrichs et al. was used, which includes polarization functions on C, N, O, and Si atoms.[28] The Stuttgart pseudopotential (SDD) was used for the lutetium atom (including 60 core electrons), with the optimized valence basis set taken from ref 29. The vibrational analysis, carried out on the optimized structures, has given all real eigenvalues for the Hessian matrix. Electronic absorption spectra were calculated by means of the time-dependent DFT formalism[30] at the corresponding ωB97X(D) optimized geometries. For the ωB97X(D) long-range corrected hybrid functional, the Coulomb term (r_{12}^{-1}) is split into a short- and long-range (with about 16 and 100% of exact exchange, respectively). It has been shown that the application of this functional improves, against the hybrid B3LYP and meta-hybrid (e.g., M06) functionals, the description of the low-lying electronic excitation energies for different tetrapyrrolic derivatives (e.g., porphyrin, chlorin).[31,32] The bulk solvent effects on excitation energies were treated within the conductor-like screening solvation model (COSMO).[33] The dielectric constant of dichloromethane (ε = 8.93) was set up along with the default cavity generation parameters. The more extended def2-SVP basis set,[34] including diffuse functions for H, C, N, O, and Si atoms, was employed for the calculation of the *in vacuo* and solution (dichloromethane and water) vertical electron affinities (VEA) and ionization potentials (IP), at the gas-phase B3LYP and PBE0 optimized geometries. The quantum-chemical calculations were carried out by means of the TURBOMOLE (for the B3LYP and PBE0 functionals) and Gaussian 03 (ωB97X and ωB97XD functionals) software packages.[35,36]

3. RESULTS AND DISCUSSION

3.1. Gas-Phase Optimized Structures. The molecular structures of the free-base iso-pentaphyrin (**1**) and its lutetium complex (**2**) have been experimentally characterized by different spectroscopic techniques (^{1}H NMR, 2D COSY, and UV−vis spectra), and their stoichiometric formulas were deduced from the mass spectrometry (ESI-MS and EI).[20] Our starting geometry follows the proposed structures by Comuzzi et al. and is reported in Figure 1. Selected optimized geometrical parameters (bond lengths and valence and torsional angles) for both **1** and **2** molecules are reported in Table 1. Their optimized structures display a highly distorted conformation, as can be shown from the dihedral angle values (Table 1) between adjacent pyrrolic rings (labeled A−E in Figure 1b). For the free base, the PBE0 torsional angle values range between 22 and 38°, with the exception of the dihedral Φ(C−E) that is about 4°. The structural differences among each functional (PBE0, B3LYP, and ωB97X) are very small, also including the sp^2 methine bridged valence angles (e.g., $C_{20}-C_{21}-C_{22}$) and the torsional angle Φ around the atom C_{11} and the substituted phenyl group. The latter Φ(C_{11}-phenyl) angle rotated by about 60°. The optimized geometrical parameters for the ωB97XD are also included in Table 1 for compound 1, and they are almost identical to the ωB97X values. For the lutetium complex (**2**), the Lu−N bond lengths are shorter for N_1-N_3 and N_5 atoms (PBE0 results: 2.272−2.381 Å)

dx.doi.org/10.1021/jp3068359 | J. Phys. Chem. B 2012, 116, 10816−10823

Table 1. Main Bond Lengths (Å), Valence and Dihedral Angles (deg) for the Lutetium Complex (2) and, in Parentheses, for the iso-Pentaphyrin Free-Base Derivative (1), Calculated at the PBE0, B3LYP, and ωB97X Levels of Theories

	PBE0	B3LYP	ωB97X
	Bond Lengths		
Lu−N_1	2.272	2.278	2.292
Lu−N_2	2.311	2.333	2.332
Lu−N_3	2.329	2.304	2.398
Lu−N_4	2.525	2.601	2.533
Lu−N_5	2.381	2.411	2.340
	Valence Angles		
C_{20}−C_{21}−C_{22}	127.9 (128.8)	128.6 (128.4)	128.1 (126.3) [126.6][a]
C_{24}−C_{26}−C_{27}	121.0 (128.4)	122.9 (131.1)	120.2 (127.2) [126.8]
C_{15}−C_{16}−C_{17}	125.6 (131.8)	126.8 (128.8)	125.9 (129.4) [129.4]
C_1−C_6−C_7	125.7 (130.2)	126.3 (128.7)	126.1 (130.0) [129.4]
C_{10}−C_{11}−C_{12}	120.5 (123.2)	119.7 (124.9)	120.8 (122.9) [123.0]
N_1−Lu−N_5	81.0	82.6	81.1
N_1−Lu−N_2	75.5	76.6	75.1
N_4−Lu−N_5	74.9	74.8	75.0
N_2−Lu−N_3	75.9	75.7	75.5
N_4−Lu−N_3	68.9	67.0	68.9
	Dihedral Angles		
Φ(C_{11}-phenyl)	48.6 (59.9)	51.3 (60.8)	52.9 (61.4) [62.0]
Φ(A-B)	25.7 (36.6)	27.1 (36.3)	25.8 (45.7)
Φ(A-C)	9.3 (29.2)	13.3 (30.6)	8.8 (31.6)
Φ(B-D)	42.0 (38.4)	39.1 (41.7)	41.2 (48.3)
Φ(C-E)	5.3 (3.8)	0.9 (10.7)	4.3 (3.2)
Φ(D-E)	32.6 (22.4)	28.2 (17.5)	31.5 (25.0)

[a]In square brackets are reported selected valence and dihedral angle values calculated at the ωB97XD/SV(P) level for compound **1**.

and slightly longer for Lu−N_4 (2.525 Å). The same trend is found for the B3LYP and ωB97X optimized geometries. For compound **2**, since the ωB97XD functional is not parametrized for lutetium atom, the optimization of this structure is not possible at this level of theory. The metal coordination lengths with the atoms N_1−N_3 are significantly reduced, with respect to the free base (**1**), the torsional angles between the corresponding pyrrolic rings are Φ(A−B) and Φ(A−C). The agreement between the computed and experimental structural parameters is quite satisfactory.

The natural atomic population and charges, derived from the NBO wave function analysis at the PBE0 level of theory, are reported in Table 2 and give some hints about the metal to ligand bond character. For the lutetium atom, the used pseudopotential assigns a $5s^2 5p^6 5d^1 6p^2$ ground-state valence configuration with 14 electrons in the f-core shell. Considering the lutetium atom in a formal charge of +3, the calculated f-orbital and d-orbital metal occupation numbers and their natural charge are 0.00, 0.48, and 2.36, respectively. This indicates a covalent metal−nitrogen bonding character, due to the partial electron donation from the pyrrolic nitrogens, whose calculated atomic charges are about −0.8. The PBE0 optimized Cartesian coordinates for compounds **1** and **2** are given in the Supporting Information.

3.2. Electronic Absorption Spectra. The spectra of porphyrins are usually rationalized through the four-orbital model proposed by Gouterman.[3,37] Mixed electronic transitions between the two highest occupied (HOMO and HOMO+1) and the two lowest unoccupied (LUMO and LUMO+1) molecular orbitals can explain the main spectroscopic features of the electronic absorption bands: the B or Soret bands (B_x and B_y) in the near-UV region and the weaker intensity Q-bands (Q_x and Q_y) in the visible or near-IR spectrum region. For expanded aromatic porphyrins, the electronic spectra similarly exhibit the strong allowed Soret band and several distinct Q-bands in the near-IR region.[4,38] The increased macrocycle size causes the bathochromic wavelength red-shift of the Q-band absorption maxima because of the π-electron delocalization. This effect is generally not linear with the number of pyrrole rings, since the structures tend to deviate from planarity and become more hindered, decreasing the electronic conjugation. The spectral features of expanded aromatic porphyrins (distinct B and Q-bands) are not present in non- or antiaromatic congeners.[39] The electronic spectrum of [24]amethyrin (an hexapyrrolic expanded porphyrin) is a representative example for this behavior showing broad absorption maxima without distinct Q-bands in the near-infrared region.[38] In this case, the electronic spectrum appearance can also be taken as a qualitative test for assigning them to be antiaromatic or aromatic compounds. The **1** and **2** antiaromatic pentapyrrolic porphyrins, reported in Figure 1, display these spectral features: broad absorption bands and no Q-bands in the near-IR region. In particular, the experimental spectrum of **1** recorded in dichloromethane solution (CH_2Cl_2) has a Soret-like band centered at 485 nm (2.56 eV, $\log \varepsilon = 4.39$) and a broad Q-band absorption wavelength maximum (λ_{max}) at 814 nm (1.52 eV, $\log \varepsilon = 3.71$).[20] The computed five lowest excitation energies, oscillator strengths, and main orbital contributions of compound **1** in CH_2Cl_2 are reported in Table 3. Since the first excitation energy (Q-band) is predicted at very low energy for both B3LYP and PBE0 exchange-correlation functionals (λ_{max} = 1340 and 1501 nm, respectively), the reported data refer to the ωB97X and ωB97XD functionals. In this case, the lowest excitation energies are found at 1.95 eV (636 nm) and 1.61 eV (770 nm), slightly overestimated in comparison with the experimental values. For the ωB97XD, the agreement with the experimental Q-band is better and smaller than 0.1 eV, though the oscillator strength is slightly weaker in comparison with the ωB97X value (0.02 vs 0.06). The Q-band absorption peak is mostly dominated by the HOMO−LUMO electronic transition with orbital contributions changing from 87% (for ωB97X) to 93% (for ωB97XD). The isodensity molecular surface plots for the most contributing molecular orbitals to

Table 2. NBO Atomic Orbital Populations (s, p, d, and f) and Atomic Charges for Lutetium and Nitrogen Atoms for Complex 2 and iso-Pentaphyrin 1 (in Parentheses), Calculated at the PBE0/SV(P) and Stuttgart Pseudopotential Level of Theory

	s		p		d		f	charge	
Lu	2.18		6.01		0.46		0.00	2.36	
N1	3.35	(3.37)	4.50	(4.24)	0.00	(0.01)	0.00	−0.86	(−0.63)
N2	3.34	(3.22)	4.47	(4.34)	0.00	(0.00)	0.00	−0.81	(−0.56)
N3	3.35	(3.37)	4.44	(4.24)	0.00	(0.01)	0.00	−0.80	(−0.62)
N4	3.32	(3.22)	4.45	(4.39)	0.00	(0.00)	0.00	−0.78	(−0.61
N5	3.36	(3.22)	4.46	(4.33)	0.00	(0.00)	0.00	−0.82	(−0.56)

dx.doi.org/10.1021/jp3068359 | J. Phys. Chem. B 2012, 116, 10816−10823

Table 3. Five Lowest Excitation Energies ΔE (eV, nm), Main Configurations, and Oscillator Strengths f for Compound 1, Calculated at the ωB97X and ωB97XD/SV(P) Levels, and for Compound 2, Calculated at ωB97X/SV(P) and Stuttgart Pseudopotential[a]

	TD-ωB97X			TD-ωB97XD		
n	$\Delta E^{b,d}$ (eV, nm)	configuration[c]	f	ΔE^{b} (eV, nm)	configuration[c]	f
			Compound 1			
1	1.95, 636	H → L (87)	0.064	1.61, 772	H → L (93)	0.027
2	3.34, 371	H − 1 → L (44) H → L + 1 (35)	1.939	3.13, 396	H → L + 1 (48) H − 1 → L (29) H − 2 → L (11)	1.897
3	3.42, 362	H → L + 2 (58) H − 2 → L (29)	1.563	3.18, 389	H → L + 2 (66) H − 2 → L (15) H − 1 → L (11)	1.400
4	3.89, 319	H → L + 1 (39) H − 1 → L (34)	0.143	3.43, 361	H − 1 → L (40) H → L + 1 (32) H − 2 → L (11)	0.079
5	4.05, 306	H − 2 → L (54) H → L + 2(26)	0.036	3.54, 350	H − 2 → L (57) H → L + 2 (21) H − 1 → L (13)	0.107
			Compound 2			
1	1.51, 820	H → L (92)	0.023			
2	3.06, 406	H → L + 1 (51) H − 2 → L (19)	1.375			
3	3.19, 389	H − 1 → L (56) H → L + 2 (24)	1.110			
4	3.49, 355	H → L + 4 (30) H → L + 6 (26) H → L + 3 (17) H → L + 2 (15)	0.040			
5	3.69, 336	H − 2 → L (50) H → L + 1 (21)	0.061			

[a]Solvent effects were included by means of the COSMO solvation model (ε = 8.93). [b]Experimental absorption peaks in dichloromethane for compound **1**: 485 nm (log ε = 4.39), 814 nm (log ε = 3.71). [c]In parentheses are reported the orbital contributions with the convention that the first number, n, refers to the occupied orbitals (HOMO − n) and the second (m) to the virtuals (LUMO + m). [d]Experimental absorption peaks in dichloromethane for compound **2**: 339 nm (log ε = 4.25), 406 nm (log ε = 4.15), 498 nm (log ε = 3.99).

excitation energies of compound **1** are reported, for the ωB97XD case, in Figure 2. The H → L electronic transition, responsible for the Q-band appearance, has a $\pi \rightarrow \pi^*$ orbital character with the electron density delocalized over all of the isopentaphyrin macrocycle. The experimental Soret-like band shows an absorption maximum at 485 nm (2.56 eV), in the near-UV region. In the case of ωB97X computations, the most intense electronic transitions ($S_0 \rightarrow S_2$ and $S_0 \rightarrow S_3$) contributing to this band are at 371 and 362 nm (f = 1.939 and 1.563), while for the ωB97XD they are found at 396 and 389 nm (f = 1.897 and 1.400). The electronic transitions are mainly made by a mixture of orbital contributions from different molecular frontier orbitals (from H − 2 to L + 2), showing that the Gouterman model is not strictly followed for this class of porphyrinoid molecules. The simulation of the electronic spectrum for compound **1** in CH_2Cl_2 (at ωB97X and ωB97XD theory level) obtained by means of a sum of Gaussian functions is reported in Figure 4 (left side). It takes into account the first 20 excitation energies and the corresponding oscillator strengths with a full width at half-maximum of 0.3 eV. The convoluted absorption peaks of the Soret-like band for the ωB97X and ωB97XD functionals are located at 368 nm (3.37 eV) and 392 nm (3.16 eV), respectively. For the corresponding lutetium(III) metal complex (**2**), the experimental UV−vis band shape in dichloromethane shows three broad absorptions at 339, 406, and 498 nm. The corresponding experimental Soret band pattern gives an absorption maximum at 480 nm. The main computed excitation energies, oscillator strengths, and main configuration, in dichloromethane, are listed in Table 3. For this compound, it was not possible to investigate the ωB97XD functional, since at present it is not parametrized for the lutetium atom. The simulated spectrum of **2** displays some analogies with the metal free molecule. The HOMO−LUMO transition, for the B3LYP and PBE0 calculations, is still present, though very weak ($f \sim 0.004$) and further red-shifted (1750 and 1890 nm) with respect to compound **1**. The corresponding ωB97X first excitation energy is at 820 nm with an oscillator strength of about 0.02, corresponding to a very weak band in the convoluted spectrum (see Figure 4, right side). The absence of the Q-band absorption in the experimental spectrum of compound **2** can be likely ascribed to the shorter lifetime of the S_1 state, enhancing so the radiationless internal conversion between the S_0 and S_1 electronic states. The ωB97X isodensity molecular surface plots for the most contributing molecular orbitals to the excitation energies of **2** are reported in Figure 4. The contribution of the metal center is evident for the L + 1 and L + 2 molecular orbitals. The Soret band stems, as for compound **1**, from the $S_0 \rightarrow S_2$ and $S_0 \rightarrow S_3$ electronic transitions having excitation energies at 3.06 and 3.19 eV, respectively. The convoluted absorption maximum is found at 398 nm (3.11 eV), differing by about 0.5 eV from the experimental value.

3.3. Photosensitization PDT Mechanisms. The combination of light, photosensitizer, and dioxygen can promote two main photochemical reactions with organic substrates (membrane

dx.doi.org/10.1021/jp3068359 | J. Phys. Chem. B 2012, 116, 10816−10823

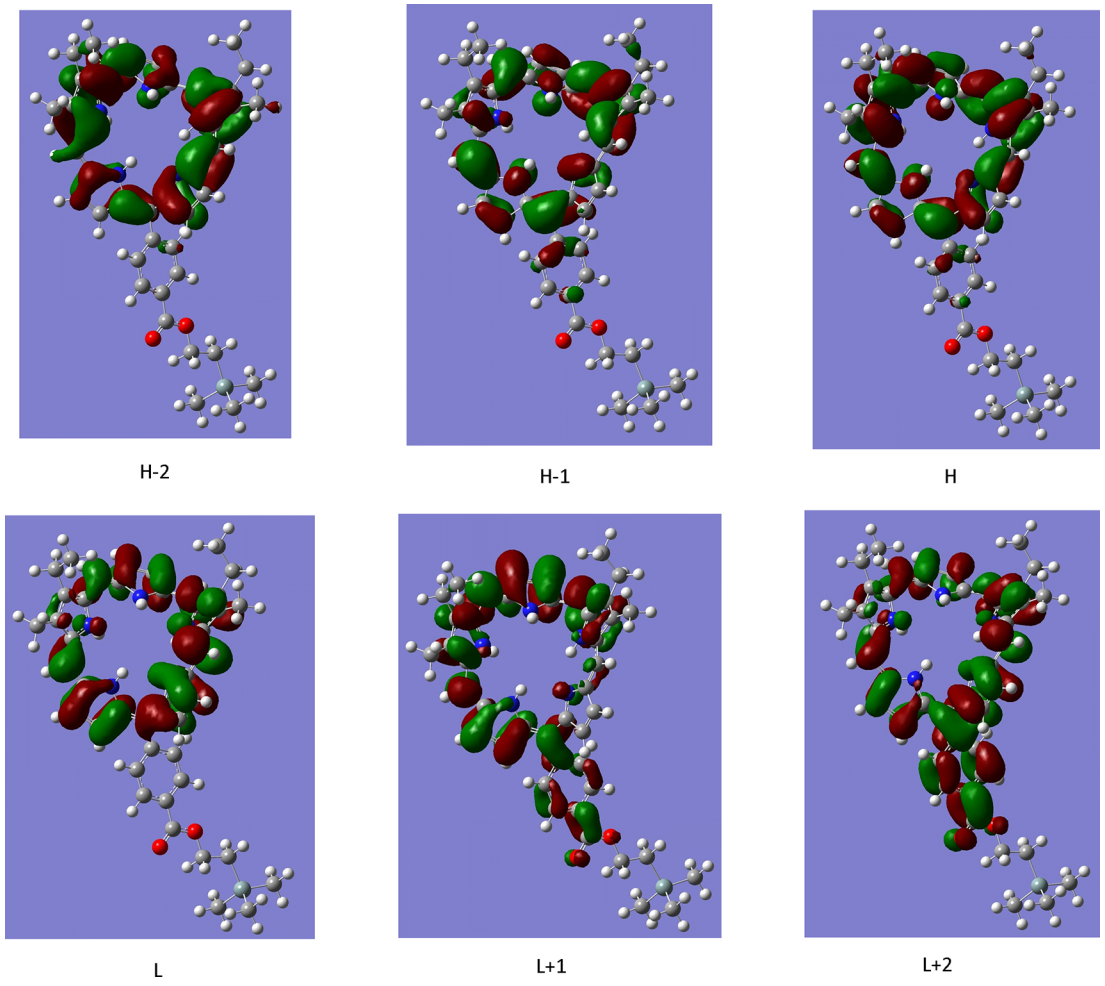

Figure 2. Frontier molecular surface plots (from HOMO − *n* to LUMO + *n*) with isodensity value of 0.02 au, for compound **1** calculated at the *ω*B97XD/SV(P) level of theory and solvent model.

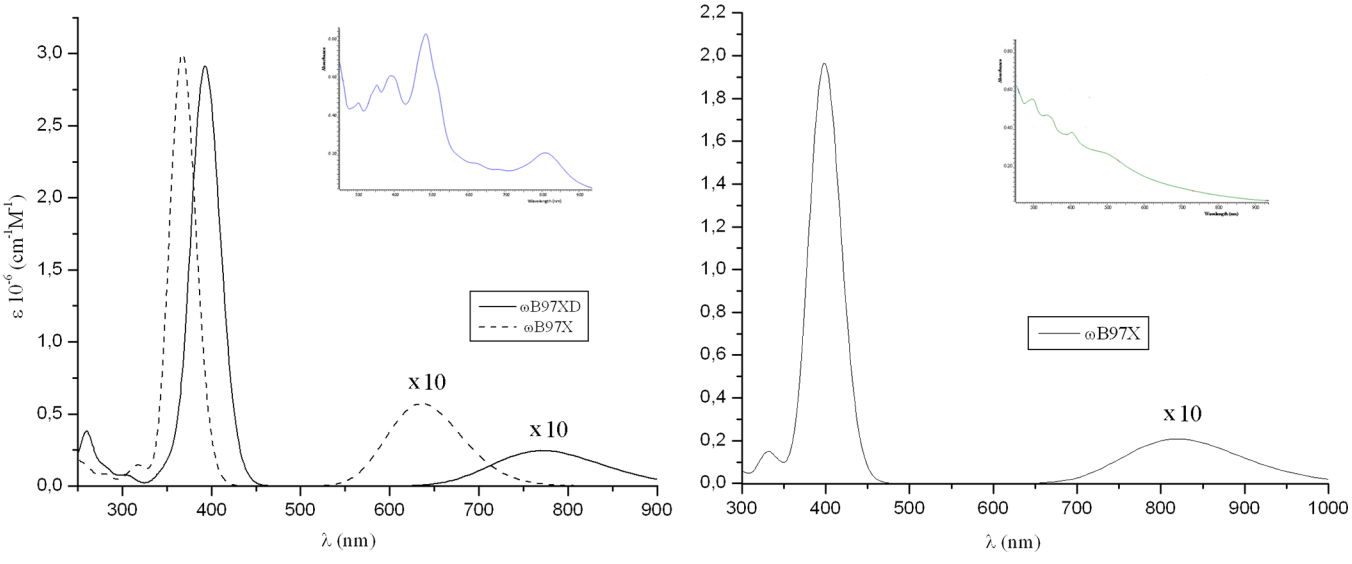

Figure 3. Simulated electronic spectra of compound **1** (left side) calculated at *ω*B97X/SV(P) (solid line) and *ω*B97XD/SV(P) (dot line) and compound **2** (right side) at *ω*B97X/SV(P)/SDD in dichloromethane. The inset shows the experimental spectra.

lipids or DNA nucleic acid bases and eventually cell damage through the generation of reactive oxygen species (ROS)). These processes, called type I and type II reaction mechanisms, will be examined together with the direct electron transfer to dioxygen and the autoionization processes, which can compete with the type I and II reactions.

3.3.1. Type I Mechanism. The oxygen-dependent type I mechanism can be outlined with a two-step reaction scheme.

dx.doi.org/10.1021/jp3068359 | *J. Phys. Chem. B* 2012, 116, 10816−10823

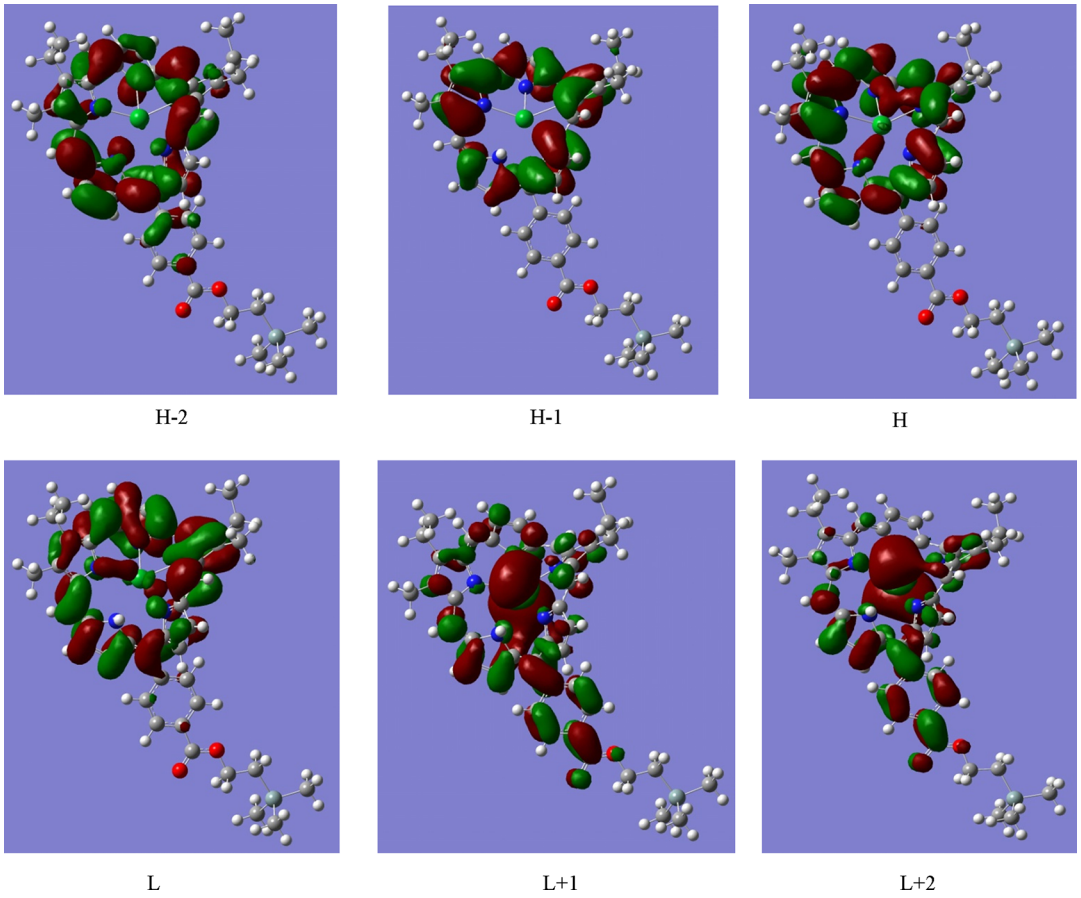

Figure 4. Frontier molecular surface plots (from HOMO − *n* to LUMO + *n*) with isodensity value of 0.02 au, for compound **2** calculated at the ωB97X/SV(P)-SDD level of theory and solvent model.

Initially (step a), the photosensitizer, in its excited triplet state (^{3}Ps*), oxidizes the substrate:

$$^3\text{Ps}^* + \text{S} \rightarrow \text{Ps}^{\bullet(-)} + \text{S}^{\bullet(+)} \quad \text{(a)}$$

Then, the reduced photosensitizer form reacts with molecular dioxygen to give the superoxide radical ion $O_2^{\bullet(-)}$ (step b):

$$\text{Ps}^{\bullet(-)} + {}^3\text{O}_2 \rightarrow {}^1\text{Ps} + \text{O}_2^{\bullet(-)} \quad \text{(b)}$$

The superoxide ion is supposed to promote indirectly the generation of ROS species by reacting with biomolecules. An important thermodynamic factor determining the energetic process, which can be computed theoretically, is given by the electron affinities of the photosensitizer in the ground (VEA) and excited triplet states (VEA(T_1)). These two parameters should be compared with the ionization potential of the substrate (step a) and that of dioxygen (step b), in order to predict if the respective reactions are energetically favorable. The vertical electron affinities of **1** and **2** were computed *in vacuo* considering two different constants (dichloromethane and water) (see Table 4) at the PBE0 and B3LYP levels of theory, since the performance of these functionals in this field has been previously tested.[40,41] The VEA values range between 1.76 and 3.23 eV (PBE0) with an increasing value in aqueous medium due to the better charge stabilization of the photosensitizer anionic form. The corresponding vertical electron affinities in the excited triplet state lie nearly in the same range 1.86−3.34 eV (PBE0), due to the small contribution of the triplet energies (E_T). The B3LYP computed electron affinities differ by almost 0.1 eV. For the ground state dioxygen, the computed adiabatic electron affinity *in vacuo* is found to be 0.34 and 0.51 eV at the PBE0/def2-SVP and B3LYP levels, respectively. The experimental value is 0.45 eV.[42] The inclusion of bulk aqueous solvation effects gives a value of 3.84 eV (3.99 eV for B3LYP). Comparing the electron affinity of dioxygen in water with the corresponding values for **1** and **2**, and supposing that the reduced photosensitizer form was generated, the reaction in aqueous solution is predicted to be favorable with an energy gain of 0.5 eV.

3.3.2. Type II Reaction Mechanism. For this mechanism, the photocytotoxic activity is caused by the reactive singlet oxygen ($^1\Delta_g$), that is generated through the energy transfer process between the photosensitizer excited lowest triplet state (Ps(T_1)) and ground state dioxygen ($^3O_2$), as follows:

$$\text{Ps}(\text{T}_1) + {}^3\text{O}_2 \rightarrow \text{Ps}(\text{S}_0) + {}^1\text{O}_2$$

The generated singlet oxygen ($^1O_2$) exerts cytotoxic effects against the cellular environment with high selectivity due to its short lifetime (4 μs).[18] To be effective, this mechanism requires that the triplet energy of the photosensitizer should be at least equal to that of $^3O_2$. For the latter, the experimental value for the electronic transition $^3O_2(^3\Sigma_g^+) \rightarrow {}^1O_2(^1\Delta_g)$ is found to be 0.98 eV.[43] From Table 4, since the triplet energies (E_T) for the investigated molecules are by far lower that the above-stated energetic limit, we can conclude that at least theoretically they cannot generate singlet oxygen. The use of the 9,10-dimethylanthracene experimental test, by Comuzzi et al.,[20] has not detected the generation of singlet oxygen after irradiation of compounds **1** and **2**, confirming in this way the too low calculated triplet energies (<0.3 eV). This evidence rules out the

dx.doi.org/10.1021/jp3068359 | J. Phys. Chem. B 2012, 116, 10816−10823

Table 4. Triplet Energies (E_T), Ground State Vertical Electron Affinities (VEA), and Ionization Potentials (VIP) for 1 and 2 Molecules, Calculated at the def2-SVPD/PBE0//def-SV(P)/PBE0 Level (B3LYP in Parentheses)[a]

Compound 1														
E_T			VEA			VEA(T_1)[b]			VIP			VIP(T_1)[c]		
$\varepsilon = 0$	$\varepsilon_{CH_2Cl_2}$	ε_{H_2O}	$\varepsilon = 0$	$\varepsilon_{CH_2Cl_2}$	ε_{H_2O}	$\varepsilon = 0$	$\varepsilon_{CH_2Cl_2}$	ε_{H_2O}	$\varepsilon = 0$	$\varepsilon_{CH_2Cl_2}$	ε_{H_2O}	$\varepsilon = 0$	$\varepsilon_{CH_2Cl_2}$	ε_{H_2O}
0.13	0.11	0.11	1.78	3.00	3.23	1.91	3.11	3.34	5.25	4.36	4.21	5.12	4.25	4.10
(0.31)	(0.29)	(0.29)	(1.64)	(2.89)	(3.12)	(1.95)	(3.18)	(3.41)	(5.21)	(4.33)	(4.18)	(4.90)	(4.04)	(3.89)
Compound 2														
E_T			VEA			VEA(T_1)			VIP			VIP(T_1)		
$\varepsilon = 0$	$\varepsilon_{CH_2Cl_2}$	ε_{H_2O}	$\varepsilon = 0$	$\varepsilon_{CH_2Cl_2}$	ε_{H_2O}	$\varepsilon = 0$	$\varepsilon_{CH_2Cl_2}$	ε_{H_2O}	$\varepsilon = 0$	$\varepsilon_{CH_2Cl_2}$	ε_{H_2O}	$\varepsilon = 0$	$\varepsilon_{CH_2Cl_2}$	ε_{H_2O}
0.10	0.13	0.13	1.76	2.93	3.14	1.86	3.06	3.27	5.11	4.18	4.02	5.01	4.05	3.99
(0.12)	(0.13)	(0.13)	(1.69)	(2.96)	(3.04)	(1.81)	(3.09)	(3.17)	(5.02)	(4.07)	(3.90)	(4.90)	(3.94)	(3.77)
Dioxygen														
VEA						VIP								
$\varepsilon = 0$		$\varepsilon_{CH_2Cl_2}$		ε_{H_2O}		$\varepsilon = 0$		$\varepsilon_{CH_2Cl_2}$		ε_{H_2O}				
0.34		3.34		3.84		12.6		9.44		8.91				
(0.51)		(3.50)		(3.91)		(12.7)		(9.49)		(8.96)				

[a]All the data, in *vacuum* and COSMO model, at different dielectric constants [ε_{H_2O} = 78.39 and $\varepsilon_{CH_2Cl_2}$ = 8.93], are reported in eV. [b]First triplet excited state electron affinities: VEA(T_1) = VEA + E_T. [c]First triplet excited state ionization potentials: VIP(T_1) = VIP − E_T.

type II mechanism as being the photochemical pathway for the high cytotoxic activity found for compound **2**.

3.3.3. Direct Electron Transfer to Dioxygen. The possible photo-oxidation of the photosensitizer, in the ground or excited state, by dioxygen, according to the following reaction

$$Ps(S_0/T_1) + {}^3O_2 \rightarrow Ps^{\bullet(+)} + O_2^{\bullet(-)}$$

can be another source for generating cytotoxic species (e.g., H_2O_2, $^\bullet$OH), after the bimolecular decay of the superoxide ion. This reaction mechanism is possible if the dioxygen is able to capture an electron from the photosensitizer, or in other terms the electron affinity of dioxygen is greater than the ionization potential of the photosensitizer. The vertical ionization potentials for **1** and **2**, for the ground (VIP) and lowest triplet excited state (VIP(T_1)), are reported in Table 4 for *in vacuo*, dichloromethane and water solution. The *in vacuo* PBE0 ionization potentials (VIP) are 5.25 and 5.11 eV for **1** and **2**, respectively (5.21 and 5.02 eV for B3LYP). The aqueous VIP values are smaller by about 0.1 eV. Considering that the electron affinity of O_2 in water, from both PBE0 and B3LYP calculations, is smaller than the studied molecules' VIPs, the reaction is not energetically feasible. However, for the lowest triplet excited state VIPs calculated at the B3LYP level, an energy gain in water solution of 0.1−0.2 eV is predicted. From Table 4, we observe that the higher ionization potential for dioxygen, *in vacuo* and water solution (>8.9 eV), in comparison with that of the pentaphyrin derivatives **1** and **2**, seems to prevent the possibility that O_2 could be oxidized by the photosensitizer.

3.3.4. Autoionization of Isopentaphyrin Derivatives. After being excited to the lowest triplet state, a photosensitizer molecule, $Ps(T_1)$, can be reduced by an identical molecule in its ground state (a) or triplet excited state (b) as follows:

$$Ps(T_1) + Ps(S_0) \rightarrow Ps^{\bullet(-)} + Ps^{\bullet(+)} \quad (a)$$

$$Ps(T_1) + Ps(T_1) \rightarrow Ps^{\bullet(-)} + Ps^{\bullet(+)} \quad (b)$$

For reaction a, the comparison between the PBE0 VEA values for the T_1 state (3.34 and 3.27 eV for **1** and **2**) and the ground state VIP ones (4.21 and 4.02 eV), computed in water, indicates that the process is endothermic and therefore not energetically favorable. This conclusion is still valid for the gas-phase and dichloromethane calculations. The autoionization process, considering both molecules lying at the first triplet excited states (reaction b), is also predicted unfavorable in the gas phase ($\varepsilon = 0$) and solutions ($\varepsilon = 8.93$ and $\varepsilon = 78.39$). The energy gain is negative (endothermic process) by more than 0.7 eV for both compounds **1** and **2** (see Table 4).

4. CONCLUDING REMARKS

The gas-phase optimized structures of the isopentaphyrin derivative **1** and its lutetium complex **2**, investigated in this work, display a high degree of distortion of the macrocycle, as can be seen from the dihedral angle value between the adjacent pyrrolic rings. This feature is basically due to the lack of electronic conjugation for these nonaromatic compounds. The main geometrical parameters derived from DFT calculations are almost similar for the exchange-correlation functionals employed for this purpose (PBE0, B3LYP, ωB97X, and ωB97XD). For the free metal isopentaphyrin, the lowest excitation energy or Q-band absorption is predicted at 772 nm with a low oscillator strength (in dicloromethane solution), by using the ωB97XD functional. The deviation error from the corresponding experimental absorption peak is about 0.1 eV. For the lutetium complex, an absorption peak in the Q-region is still predicted very weak, though it does not appear in the experimental spectrum. The triplet energies of these compounds are smaller than 0.3 eV, ruling out the ability to generate singlet oxygen by means of a type II PDT mechanism. Other mechanisms (type I mechanism and direct electron transfer to O_2), which can form reactive and cytotoxic oxygen species, have been analyzed by computing the energy gain for the model reaction. In particular, considering the energetic parameters involved in the type I mechanism (electron affinities and ionization potentials), the reaction is predicted energetically possible (exothermic process), in a solution simulating the water dielectric constant.

dx.doi.org/10.1021/jp3068359 | J. Phys. Chem. B 2012, 116, 10816−10823

■ ASSOCIATED CONTENT

Supporting Information

In vacuo optimized Cartesian coordinates for compounds **1** and **2** calculated at the PBE0/SV(P) level. This material is available free of charge via the Internet at http://pubs.acs.org.

■ AUTHOR INFORMATION

Corresponding Author

*Phone: +39-0984-492048. Fax: +39-0984-492044. E-mail: nrusso@unical.it.

Notes

The authors declare no competing financial interest.

■ ACKNOWLEDGMENTS

Financial support from the Università degli Studi della Calabria and MIUR (PRIN 2008) is gratefully acknowledged.

■ REFERENCES

(1) Dolphyn, D. *The Porphyrins*; Academic Press: New York, 1978; Vol. *I*.
(2) Falk, J. E. *Porphyrins and Metalloporphyrins*; Elsevier: Amsterdam, The Netherlands, 1964.
(3) Gouterman, M. *J. Mol. Spectrosc.* **1961**, *6*, 138−163.
(4) Saito, S.; Osuka, S. A. *Angew. Chem., Int. Ed.* **2011**, *50*, 4342−4373.
(5) Jasat, A.; Dolphin, D. *Chem. Rev.* **1997**, *97*, 2267−2340.
(6) Woodward, R. B. *Aromaticity: An International Symposium*, Sheffield, U.K., 6-9 July, 1966; Special publication no. 21; The Royal Chemical Society: London, U.K., 1966.
(7) Bauer, V. J.; Clive, D. L. J.; Dolphyn, D.; Paine, J. B.; Harris, F. L.; King, M. M.; Loder, J.; Wang, S. W. C.; Woodward, R. B. *J. Am. Chem. Soc.* **1983**, *105*, 6429−6436.
(8) Sessler, J. L.; Seidel, D. *Angew. Chem., Int. Ed. Engl.* **2003**, *42*, 5134−5175.
(9) Franck, B.; Nonn, A. *Angew. Chem., Int. Ed. Engl.* **1995**, *34*, 1795−1811.
(10) Sessler, J. L.; Hemmi, G.; Mody, T. D.; Murai, T.; Burrell, A.; Young, S. W. *Acc. Chem. Res.* **1994**, *27*, 43−50.
(11) Young, S. W.; Qing, F.; Harriman, A.; Sessler, J. L.; Dow, W. C.; Mody, T. D.; Hemmi, G. W.; Hao, Y.; Miller, R. A. *Proc. Natl. Acad. Sci. U.S.A.* **1996**, *93*, 6610−6615.
(12) Ahn, T. K.; Kwon, J. H.; Kim, D. Y.; Cho, D. W.; Jeong, D. H.; Kim, S. K.; Suzuki, M.; Shimizu, S.; Osuka, A.; Kim, D. *J. Am. Chem. Soc.* **2005**, *127*, 12856−12861.
(13) Sessler, J. L.; Cyr, M.; Furuta, H.; Král, V.; Mody, T.; Morishima, T.; Shionoya, M.; Weghorn, S. *Pure Appl. Chem.* **1993**, *65*, 393−398.
(14) Burrell, A. K.; Hemmi, G.; Lynch, V.; Sessler, J. L. *J. Am. Chem. Soc.* **1991**, *113*, 4690−4692.
(15) Sessler, J. L.; Tomat, E. *Acc. Chem. Res.* **2007**, *40*, 371−379.
(16) Bonnett, R. *Chemical Aspects of Photodynamic Therapy*; Gordon & Breach Science Publishers: Amsterdam, The Netherlands, 2000.
(17) O' Connor, A. E.; Gallagher, W. M.; Byrne, A. *Photochem. Photobiol.* **2009**, *85*, 1053−1074.
(18) Ogilby, P. *Chem. Soc. Rev.* **2010**, *39*, 3181−3209.
(19) Turro, N. J. *Modern Molecular Photochemistry*; Benjamin: Menlo Park, CA, 1978.
(20) Ballico, M.; Rapozzi, V.; Xodo, L. E.; Comuzzi, C. *Eur. J. Med. Chem.* **2011**, *46*, 712−720.
(21) Becke, A. D. *J. Chem. Phys.* **1993**, *98*, 5648−5652.
(22) Adamo, C.; Barone, V. *J. Chem. Phys.* **1999**, *110*, 6158−6170.
(23) Ernzerhof, M.; Scuseria, G. E. *J. Chem. Phys.* **1999**, *110*, 5029−5036.
(24) Chai, J. D.; Head-Gordon, M. *J. Chem. Phys.* **2008**, *128*, 84106−84155.
(25) Chai, J. D.; Head-Gordon, M. *Phys. Chem. Chem. Phys.* **2008**, *10*, 6615−6620.
(26) Jacquemin, D.; E. Perpete, E. A.; Ciofini, I.; Adamo, C. *Acc. Chem. Res.* **2009**, *42*, 326−334.
(27) Send, R.; Kühn, M.; Furche, F. *J. Chem. Theory Comput.* **2011**, *7*, 2376−2386.
(28) Schäfer, A.; Horn, H.; Ahlrichs, R. *J. Chem. Phys.* **1992**, *97*, 2571−2577.
(29) Cao, C. X.; Li, Q.; Moritz, A.; Xie, Z.; Dolg, M.; Chen, X.; Fang, W. *Inorg. Chem.* **2006**, *45*, 3444−3451.
(30) Casida, M. E. In *Recent Developments and Applications in Density-Functional Theory*; Seminario, J. M., Eds.; Elsevier: Amsterdam, The Netherlands, 1996; pp 155−192.
(31) Tian, B.; Eriksson, E. S. E.; Eriksson, L. A. *J. Chem. Theory Comput.* **2010**, *6*, 2086−2094.
(32) Eriksson, E. S. E.; Eriksson, L. A. *Phys. Chem. Chem. Phys.* **2011**, *13*, 7207−7217.
(33) Klamt, A.; Schüürmann, G. *J. Chem. Soc., Perkin Trans. 2* **1993**, *5*, 799−805.
(34) Rappoport, D.; Furche, F. *J. Chem. Phys.* **2010**, *133*, 134105−134111.
(35) Ahlrichs, R.; Bär, M.; Häser, M.; Horn, M.; Kölmel, C. *Chem. Phys. Lett.* **1989**, *162*, 165−169.
(36) Frisch, M. J.; Trucks, G. W.; Schlegel, H. B.; Scuseria, G. E.; Robb, M. A.; Cheeseman, J. R.; Montgomery, J. A., Jr.; Vreven, T.; Kudin, K. N.; Burant, J. C.; et al. *Gaussian 03*, revision C.02; Gaussian, Inc.: Wallingford, CT, 2004.
(37) Gouterman, M.; Wagnière, G. H.; Snyder, L. C. *J. Mol. Spectrosc.* **1963**, *11*, 108−127.
(38) Shin, J-Y; Kim, K. S.; Yoon, M-C; Lim, J. M.; Yoon, Z. S; Osuka, A.; Kim, D. *Chem. Soc. Rev.* **2010**, *39*, 2751−2767.
(39) Yoon, M-C; Cho, S.; Suzuki, M; Osuka, A.; Kim, D. *J. Am. Chem. Soc.* **2009**, *131*, 7360−7367.
(40) Guedes, R. C.; Eriksson, L. A. *Photochem. Photobiol. Sci.* **2007**, *6*, 1089−1096.
(41) Quartarolo, A. D.; Chiodo, S. G.; Russo, N. *J. Comput. Chem.* **2011**, *33*, 1091−1100.
(42) Travers, M. J.; Cowles, D. C.; Ellison, G. B. *Chem. Phys. Lett.* **1989**, *164*, 449−455.
(43) Herzberg, G. *Spectra of Diatomic Molecules*, 2nd ed.; Van Nostrand Reinhold: New York, 1950.